Graphical Abstract

A Mn(II) complex of boradiazaindacene (BODIPY) loaded graphene oxide as both LED light and H_2O_2 enhanced anticancer agent

Xiao-Lei Xu, Jian Shao, Qiu-Yun Chen*, Cheng-Hao Li, Meng-Yun Kong, Fang Fang, Ling Ji, Daniel Boison, Tao Huang, Jing Gao, Chang-Jian Feng

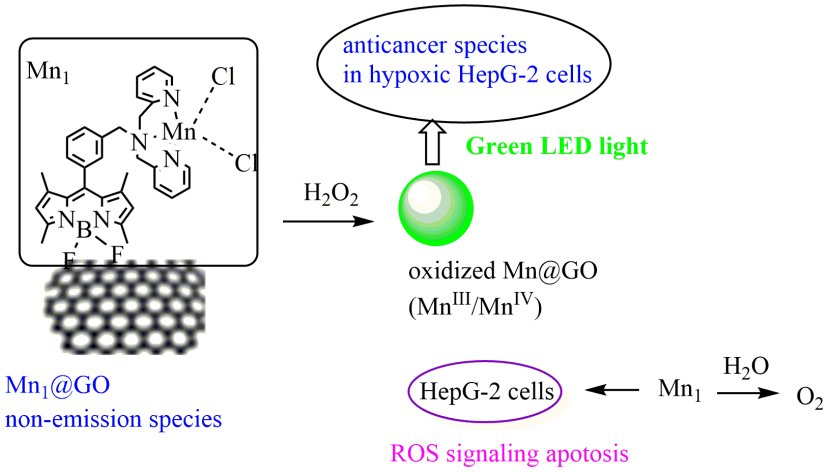

A Mn(II) complex of boradiazaindacene (BODIPY) loaded graphene oxide as both LED light and H_2O_2 enhanced anticancer agent

Xiao-Lei Xu [a], Jian Shao [a], Qiu-Yun Chen [*a, b], Cheng-Hao Li [a], Meng-Yun Kong [a], Fang Fang [a], Ling Ji [a], Daniel Boison [b], Tao Huang [b], Jing Gao [b], Chang-Jian Feng [c]

[a] *School of Chemistry and Chemical engineering, Jiangsu University, Zhenjiang, 212013, P. R. China. Tel.: +86 0511 8879800; Fax: +86 0511 88791602;*

[b] *School of Pharmacy, Jiangsu University, Zhenjiang, 212013, P.R. China*

[c] *College of Pharmacy, University of New Mexico, Albuquerque, New Mexico 87131, USA*

Corresponding author

*Tel.: +86 0511 8879800; Fax: +86 0511 88791602; School of Chemistry and Chemical engineering, Jiangsu University, Zhenjiang, 212013, P. R. China.

*E-mail address: chenqy@ujs.edu.cn (Q.Y. Chen)

ABSTRACT

Cancer cells are more susceptible to H_2O_2 induced cell death than normal cells. H_2O_2-activatable and O_2-evolving nanoparticles could be used as photodynamic therapy agents in hypoxic environments. In this report, a photo-active Mn(II) complex of boradiazaindacene derivatives (Mn_1) was used as a dioxygen generator under irradiation with LED light in water. Moreover, the in vitro biological evaluation for Mn_1 and its loaded graphene oxide (herein called Mn_1@GO) on HepG-2 cells in normal and hypoxic conditions has been performed. In particular, Mn_1@GO can react with H_2O_2 resulting active anticancer species, which show high inhibition on both HepG-2 cells and $CoCl_2$-treated HepG-2 cells (hypoxic cancer cells). The mechanism of LED light enhanced anticancer activity for Mn_1@GO on HepG-2 cells was discussed. Our results show that Mn(II) complexes of boradiazaindacene (BODIPY) derivatives loaded GO can be both LED light and H_2O_2-activated anticancer agents in hypoxic environments.

Keywords. Manganese; Cancer; H_2O_2-activatable; Photodynamic; Graphene

1. Introduction

Photodynamic therapy (PDT) is a clinical modality that employs a photosensitizer, an appropriate excitation light, and oxygen (O_2) molecules to generate cytotoxic singlet oxygen ($^1O_2$) for the treatment of cancers [1]. Although PDT has become a promising treatment option for early stage cancer and an adjuvant for surgery in late-stage cancer, tumor hypoxia severely reduce the therapeutic efficiency [2]. Hypoxia is increasingly being recognized as a characteristic feature of solid tumors. The photosensitizer-mediated consumption of O_2 during PDT further potentiates tumor hypoxia. Thus, the application of traditional PDT agents is significantly limited by the tumor hypoxia due to the O_2-dependent nature of PDT [3]. Thus, it is urgent to develop non-dioxygen dependent PDT agent [4]. Cellular levels of H_2O_2 directly or indirectly play a key role in malignant transformation and in sensitizing cancer cells to death. During the overexpression of H_2O_2 detoxifying enzymes or catalase in vivo, H_2O_2 concentration was expected to decrease, and the cancer cells reverted to normal appearance [5]. Cancer cells are more susceptible to H_2O_2 induced cell death than are normal cells. Mn(II) complexes of N-substituted di(picolyl)amines have been reported as mimics of catalase. For example, manganese(II) complexes of N-substituted di(picolyl)amines have been found to be multifunctional complexes that could act as mimics of catalase that inhibit the proliferation of cancer cells by attenuating the absorption of Ca^{2+} in mitochondria as well as disproportionation of H_2O_2 [6]. Recently, we found that [Mn(Adpa)(Cl)(H_2O)] (Adpa=bis(pyridyl-methyl)amino-2-propionic acid) exhibited anti-proliferative and cytotoxic activity against diverse tumor types in vitro, as well as against tumor xenografts mediated by the ROS-dependent apoptotic and autophagic cell death [7]. Hence, Mn(II) complexes could be H_2O_2 activated anticancer

complexes. H_2O_2-activatable and O_2-evolving complexes could be used as clinical therapy agents in hypoxic environments.

Boradiazaindacenes (BODIPY) are very popular fluorophores with high quantum yields, long-wavelength absorption and fluorescence emission in the visible spectral region [8]. BODIPY derivatives are used as fluorescence tags and probes which function in water or organic solvent, and near-IR absorbing BODIPY derivatives can be glutathione-activated photosensitizers for photodynamic therapy [9]. Previously, we found that BODIPY based cobalt(II) complexes could react with water to generate $^1O_2$ using water as the oxygen source [10]. It is therefore possible that Mn(II) complexes of BODIPY can be light activated anticancer agents. Graphene oxide (GO) is a combination of sp^2 and sp^3 hybridized carbon atoms and has remarkable optical properties. Hydrophobic organic compounds have been loaded on to the functional GO via stacking and hydrophobic interactions to increase the specific target to breast cancer cells [11]. Thus, the assembly of GO with photoactive Mn(II) complexes could increase the cancer target. Here, we report the LED light driven water oxidation and anticancer property of [(BDA)$MnCl_2$] (Mn_1) and its loaded graphene oxide (Mn_1@GO) (BDA = 8-[di(2-picolyl)amine-3-benzyl]-4,4-difluoro-1,3,5,7-tetramethyl-4-bora-3a,4a-diaza-s-indacen)) (Scheme 1).

(Scheme 1)

2. Experimetal section

2.1 Materials and methods.

8-[Di(2-picolyl)amine-3-benzyl]-4,4-difluoro-1,3,5,7-tetramethyl-4-bora-3a,4a-diaza-s-indacene (BDA) was synthesized as reported [12]. The C, H and N microanalyses were

performed on a Vario EL elemental analyzer. The metal analysis was recorded on TAS-986 atomic absorption spectrophotometer. Electronic absorption spectra were recorded in the 900-190 nm region using a Varian CARY 50-BIO UV-VIS spectrophotometer. Infrared spectra were recorded on a Nicolet-470 spectrophotometer in the wavenumber range of 4000-400 cm^{-1} using KBr pellets. Fluorescence measurements were performed on a fluorescence spectrofluorometer Model CARY Eclipse (VARIAN, USA), a 1.0 cm quartz cell (ex= 460 nm, slit width = 5 nm).The electrospray mass spectra (ES-MS) were determined on a Finnigan LCQ mass spectrograph. TEM was performed at room temperature on a JEOL JEM-200CX transmission electron microscope using an accelerating voltage of 200 kV. The EPR spectra of complexes in CH_3CN were acquired at 298 K with a 0.201 mW power, 0.5 G modulation amplitude, and 100 kHz modulation frequency. The volume of O_2 was measured by direct methods, via connecting of the reaction vessel with a U-tube to a calibrated microburet with collection of the gas released. Oxygen evolution was monitored by gas chromatography using a thermal conductivity detector (GC-TCD).

2.2 Synthesis of [(BDA)$MnCl_2$] (Mn_1)

A solution of BDA (100 mg, 0.186 mmol) in 15 ml C_2H_5OH was mixed with $MnCl_2 \cdot 4H_2O$ (37 mg, 0.186 mmol).The mixture was refluxed for 2 h at 70℃, and then it was cooled to room temperature to give brown red solution. After recrystallized with $CH_3CH_2OCH_2CH_3$-CH_3CN (1:1), red solid (103 mg) was obtained yield 84%. Found: C, 57.89; H, 4.85; N, 10.58, Mn, 8.24. Calcd. (%) for $C_{32}H_{32}BCl_2MnF_2N_5$: C, 58.12; H, 4.88; N, 10.59, Mn 8.31. UV-vis(CH_3CN/nm) ($\varepsilon \times 10^{-4}$, M^{-1} cm^{-1}): 231 (3.2), 262 (1.6), 315 (1.1), 362(1.1), 498 (7.7). IR(KBr, ν/cm^{-1}): 3391 m, 2963-2923 m, 1605 m, 1543 s, 1303 s, 1195 s, 981 s, 747 m. The metal analysis and elemental

analysis indicate that the ratio of ligand (BDA): metal in Mn_1 is 1:1. The thermal analysis (TG) curve of Mn_1 in the range 0–1000 °C is shown in Fig. S1. The main peak for Mn_1 in MeCN m/z(%) = 625.27 (100) corresponds to the species $[(BDA)MnCl]^+$ (Fig. S2).

2.3 Synthesis of Mn_1@GO (GO= Graphene oxide)

GO (2 mg) was dispersed to water (2 mL) resulting a dispersed solution of GO (2 mg/mL). The dispersed solution of GO (2 mL, 2 mg/mL) was added to the solution (3 mL, H_2O: DMSO = 9:1) of Mn_1(100 μM). After the mixture was vigorously shaken for 1.5 h at room temperature, CH_3CN (5 mL) was added to precipitate the product. After centrifugation, the precipitate was washed with CH_3CN to remove the free Mn_1. The product Mn_1@GO was obtained after it was dried in vacuum.

2.4 Cytotoxicity testing

The cytotoxicity assays were measured with HepG-2 cells in normal culture conditions. HepG-2 cells were seeded at adensity of 4×10^4 cells ml^{-1} into sterile 96-well plates. The complex Mn_1 and Mn_1@GO were added in DMSO and diluted with culture media. After 24 h, Mn_1 and Mn_1@GO were added into the cultured HepG-2 cells for 24 h. Cell viability was determined by the 3-[4,5-dimethylthiazol-2-yl]-2,5-diphenpyltetra-zolium bromide (MTT) assay measuring the absorbance at 570 nm. Each test was performed in triplicate. Morphological change of HepG-2 cells was taken using Nikon Ti-E2000 microscope with live cell system.

2.5 Cell morphological changes

The morphological changes of the H_2B-GFP-labeled HepG-2 cells were observed under a Nikon TE2000 microscope (Nikon, Tokyo, Japan) with a live cell system (LCS) which can

provide CO_2, temperature control and position fixing. The H_2B-GFP-labeled HepG-2 cells, which were incubated with materials, were observed for 24 h. The bright and fluorescence imaginations of the cells were recorded and analyzed.

2.6 Measurement of intracellular ROS production

The intracellular generation of ROS was analyzed using the probe, DCFH-DA. Cells were incubated with 10 μM DCFH-DA at 37 ˚C for 15 min. The DCF fluorescence distribution of 1×10^4 cells was then measured by fluorescence spectrometry (Spectra Max Gemini; Molecular Devices Corp.).

2.7 Mitochondrial imaging

HepG-2 cells were cultured in RPMI-1640 medium and DMEM medium (Gibco, USA), supplemented with 10% (v/v) heat-inactivated fetal bovine serum and antibiotics (100 U. $\cdot$ ml^{-1} penicillin and 100 U $\cdot$ ml^{-1} streptomycin) at 37 ^{0}C in a humidified atmosphere of 5% CO_2. HepG-2 cells (2.4×10^4) were seeded into 24-well plates (every plate was 100 ml) for 24 h. Complexes were dissolved in DMSO and diluted with culture media then added and incubated for 1 h. Next, the cells were dyed with 1 mg $\cdot$ ml^{-1} MitoTracker Red FM (Molecular Probes Corporation, USA) for another 1h. Cell imaging of HepG-2 cells was conducted using a Nikon Ti-E 2000 microscope with live cell system (LCS) which can provide CO_2, temperature control and position fixing. The brightness and fluorescence imaging of cells were recorded.

2.8 JC-1 staining to measure mitochondrial membrane potentials (MMP)

MMP was determined using the fluorescent dye JC-1. HepG-2 cells were seeded in 96-well plates or on chamber slides and treated with complexes at the indicated concentrations and times. Fluorescence intensity was measured immediately following JC-1 staining (5 mg · mL^{-1} of JC-1 at 37°C for 30 min) by fluorescence spectrometry (Molecular Devices Corporation, USA) or observed using a fluorescence microscope (excitation 488 nm/emission 595 nm for JC-1 red).

2.9 Western blot analysis on expression level of HIF-1α in HepG-2 cells

Proteins were extracted in lysis buffer (30 mM Tris, pH 7.5, 150 mM sodium chloride, 1 mM phenylmethanesulfonyl fluoride, 1 mM sodium orthovanadate, 1% Nonidet P-40, 10% glycerol, and phosphatase and protease inhibitors), separated by SDS-PAGE and transferred onto polyvinylidene fluoride membranes. The membranes were probed with antibodies (HIF-1α and β-actin) overnight at 4˚C, and then incubated with a horse radish peroxidase-coupled secondary antibody. Detection was performed using a LumiGLO chemiluminescent substrate system [Kirkegaard & Perry Laboratories, Inc. (KPL), Gaithersburg, MD, USA].

3. Results and Discussions

3.1 Photophysical properties of Mn_1 and Mn_1@GO.

The UV spectra of Mn_1 had bands at 230, 265, 315, 360, 460 nm and 499 nm (Fig. 1). The band at 460 nm and 499 nm can be attributed to the π-π* transition of the BODIPY structure. The wider band at 315 nm and 360 nm in Mn_1 confirms the metal-ligand charge transfer interaction. The fluorescence spectrum of Mn_1 presents a strong emission at 508 nm when excited at 460 nm (Fig. 2). The positive charged complex Mn_1 can interact with GO via

electrostatic and π–π stacking. Adding GO to the solution of Mn_1 leads to the decreased emission at 508 nm until the emission quenched completely when the ratio of Mn1 and GO is 1 μM : 5 μg (1 mM Mn_1/g GO). The band at 499 nm of Mn_1@GO can be attributed to the π-π* transition of BODIPY structure, indicating that Mn_1 has been combined to GO successfully. According to the TEM image of Mn_1@GO, we found that Mn_1 was wrapped in GO and nanospheres with the size of ca. 120-220 nm were formed (Fig. 3).

Fig. 1. UV spectra of BDA (a, 10 μM), Mn_1 (b, 10 μM), GO (c, 28 μg·mL^{-1}) and Mn_1@GO (d, C_{Mn1} 6 μM, C_{GO} 30 μg·mL^{-1}) in MeCN-H_2O (v:v = 2:1).

Fig. 2. Fluorescence spectra of Mn_1 (1.5 μM, DMSO) in the presence of various amount of GO (m_{GO}= 0, 20, 40, 60, 80, 100, 120, 140, 160, 180 μg). The excitation wavelength was 460 nm.

Fig.3.TEM image of GO (left) and Mn_1@GO (right).

3.2 Water oxidation catalyzed by Mn_1

The complex catalyzed water oxidation was confirmed by measuring the green LED light (500-600 nm, 10 w) irradiated due to the oxygen evolution. The obvious oxygen bubble could be observed when the complex Mn_1 was added to H_2O solution (Fig. 4, Table S1) while Mn_1@GO showed little activity of water oxidation. The complex was active at pH 7.2 with the turnover frequency (TOF) of Mn_1 22.68 h^{-1}. When the reaction was carried out in dark, nearly no oxygen evolution could be monitored, and we deduced that the reaction was light driven oxidation of water. The initial rate was measured as function of catalyst Mn_1 concentration. The initial rate of

O_2 evolution was plotted as a function of the concentration of Mn_1 giving a first-order rate constant k_1 of 0.027±0.002 min^{-1} at 25 ºC, pH 7.2 (Fig. 4 b).

Fig.4. a) O_2 production from an aqueous solution containing Mn_1 (2 mg) under green LED light(500-600 nm, 10 W) at different pH (☆, aqueous phosphate buffer (PB) solution, pH 7.2; ◆, H_2O; ▲, PB solution, pH 8.5; ○, PB solution, pH 4.0); b) The initial rate of O_2 evolution plotted as a function of the concentration of Mn_1. Slop =0.027±0.002 min^{-1}, R^2=0.980.

The interaction of Mn_1 and water was monitored by UV-vis spectroscopy (Fig. S3). A new absorbance at 560 nm emerged when Mn_1 was titrated with water. This suggested that the reaction of Mn_1 with H_2O could result in the formation of oxidized complex intermediates. Recycled Mn_1 was obtained after Mn_1 reacted with water for 1 h, centrifuged and dried in vacuum. The EPR spectra of recycled Mn_1 in MeCN show multiline EPR signals at g = 4.1 indicating existence of Mn^{III} or Mn^{IV} (Fig. 5) [13]. Hence, we deduce that the in-site formed Mn^{III} or Mn^{IV} intermediates can work as electron acceptors because Mn_1 can catalyze water oxidation without extra electron acceptors. For water oxidation, the recycled Mn_1 is less active than Mn_1. Only Mn_1-H_2O system is a dioxygen generator.

Fig. 5. X-Band EPR spectrum of recycled Mn_1 in MeCN

3.3 Electrochemical properties.

In dry MeCN solution at a pt electrode, the Mn_1 displays one irreversible Mn^{III}/Mn^{II} couple at $E_{1/2}$ = -0.3 V and one quasi-reversible redox couple at 1.62 V, which can be assigned to the

oxidation of ligand (Figure S4). The Mn_1@GO (dispersed in dry MeCN) displays one irreversible redox peak at -0.35 V. With the addition of water, a reversible Mn^{V}/Mn^{IV} wave at 1.05 V was observed for Mn_1@GO in MeCN:H_2O = 6:1 solution (Fig. 6). This indicates that Mn_1@GO (Mn^{2+}) can react with water resulting oxidized Mn_1@GO (Mn^{n+}, n = IV or V) in electrochemical conditions. Moreover, titration of Mn_1@GO with equal amount of H_2O_2 results oxidized Mn_1@GO (labeled as Mn_1@GO@H_2O_2). The redox peak at 0.51 V indicates the main species for Mn_1@GO@H_2O_2 in MeCN-H_2O (1:1) solution are Mn^{IV}/Mn^{III} couples (Fig. S5). Electrochemical data confirm that Mn_1@GO can react with H_2O_2 resulting oxidized manganese species.

Fig. 6. Cyclic voltammetry curves of solutions of Mn_1@GO (C_{Mn}, 1mM) in dry MeCN (black line), Mn_1@GO in MeCN:H_2O = 6:1 (dashed line) at 298 K (vs SCE), platinum working electrode, 100 mV/s scan rate.

3.4 Cytotoxicity assay

Mn_1 and Mn_1@GO were studied for their antitumor activity in vitro by determining their inhibition against growth of HepG-2 cells using the method of MTT reduction. Both Mn_1 and Mn_1@GO were active against HepG-2 cells in dose dependent manner with IC_{50} values of 10.45 μM (C_{Mn1}) and 10.14 μM (C_{Mn2+}), respectively (Fig. 7). To explore the anticancer activity for Mn_1 and Mn_1@GO in hypoxic conditions, the HepG-2 cells were incubated with $CoCl_2$ (200 μM) for 24 h, and then cell viability was examined by MTT. It is found that Mn_1@GO@H_2O_2 ($C_{Mn2+,}$ 4 μM) show good inhibition on $CoCl_2$ treated HepG-2 cells, the inhibition for Mn_1 and Mn_1@GO on the proliferation of $CoCl_2$ treated HepG-2 cells is dependent on their

concentrations (Fig. S6). This indicates that dioxygen concentration has great effect on the anticancer activities of Mn_1 and Mn_1@GO. Cellular levels of H_2O_2 directly or indirectly play a key role in malignant transformation and sensitizing cancer cells to death [5]. Cancer cells are more susceptible to H_2O_2 induced cell death than normal cells are. H_2O_2 is considered to be a mediator of apoptotic cell death [14]. Based on the reaction of Mn_1@GO with H_2O_2, we deduce that Mn_1@GO can be as potential H_2O_2 activated anticancer materials.

Fig. 7. Inhibition activities of Mn_1 and Mn_1@GO on the proliferation of HepG-2 cells. HepG-2 cells without compounds were used as controls.

To study whether Mn_1 and Mn_1@GO could be used as photo-activated anticancer agents, HepG-2 cells were treated with Mn_1 (1 μM) or Mn_1@GO (C_{Mn1}, 1 μM) in dark and green LED light irradiated conditions, and the cells were analyzed (Fig. S7). The HepG-2 cells without drugs were used as the control. Mn_1 (1 μM) or Mn_1@GO (C_{Mn1}, 1 μM) was used since it showed nearly no inhibition on the proliferation of HepG-2 cells in the dark so that every inhibition may be due to its activation upon the irradiation of the LED light. Control experimental results showed HepG-2 cells show nearly no cell shrinkage when irradiated by green LED (10 w) light for 15 min. We also found that both Mn_1 (1μM) or Mn_1@GO (C_{Mn1}, 1 μM) could cause obvious death of HepG-2 cells when irradiated for 15 min, while cells showed normal morphology when treated with Mn_1 (1 μM) or Mn_1@GO (C_{Mn1}, 1 μM) without green LED light. This result demonstrates that both Mn_1 (1 μM) and Mn_1@GO (C_{Mn1}, 1 μM) could act as potential photo-activated anticancer agents. The LED light enhanced anticancer property for Mn_1 may be due to the ability of Mn_1 to catalyze the water oxidation with the generation of dioxygen thereby

increasing the amount of oxygen in the cell. This increased oxygen lead to increased amount of singlet oxygen ($^1O_2$), $^{\cdot}OH$ and other intermediates when LED light was incident on Mn_1, which could induce cell death and oxidative stress. This was confirmed by the high ROS production (Fig. 8) which may induce apoptotic cell death. This shows that the amount of the oxygen in the cancer cells plays a critical role in the photosensitization therapy.

From Fig. 8, though both Mn_1 and Mn_1@GO exerted antitumor activity through production of high concentration of ROS when irradiated, the ROS produced by Mn_1 was about two times that of Mn_1@GO. This suggests that conversion of H_2O_2 into oxygen plays very important role in the ROS production during the light irradiation. Mn_1@GO showed little activity in the oxygen production therefore depended on the only oxygen in cell for the sensitization thereby inducing lower amount of ROS. Mn_1@GO can react with H_2O_2 with the emission at 508 nm partially recovered (Fig. S8) and Mn_1@GO mixed with H_2O_2 in water resulting in Mn_1@GO@H_2O_2, which have a redox peak at 0.51 V indicating the existence of the Mn^{IV}/Mn^{III} species in Mn_1@GO@H_2O_2. EPR data of Mn_1@GO@H_2O_2 nanoparticles show the multiline EPR signals at g = 4.6 (Fig. S9). These indicate that Mn_1@GO may react with H_2O_2 and produce intermediates Mn_1@GO@H_2O_2, which show high inhibition on both HepG-2 cells and $CoCl_2$–treated signaling HepG-2 cells. The reaction of Mn_1@GO and H_2O_2 with the formation of Mn_1@GO@H_2O_2 can be accelerated by LED light. Thus, the anticancer of Mn_1@GO also can be enhanced by LED light. Above all, Mn_1@GO can be LED light enhanced anticancer materials in hypoxic environments.

Fig. 8. Effect on the ROS content in HepG-2 for Mn_1 (1 μM) and Mn_1@GO (C_{Mn1}, 1 μM).

3.5 Target mitochondrial and effect on the expression of HIF

The mitochondrial target imaging of Mn_1 was assessed by comparison with Mito Tracker Red FM. MitoTracker Red FM binds to lipids in mitochondria membranes. HepG-2 cells were incubated with Mn_1 (10 μM) for 60 min at 37 ℃, then MitoTracker Red FM (1 $mg \cdot mL^{-1}$) was added, and the cell images were recorded. The green fluorescence is overlapped with red emission of MitoTracker Red FM indicating that Mn_1 can enter the mitochondrial in HepG-2 cell (Fig. 9). To examine whether the Mn_1 and Mn_1@GO can affect mitochondrial function, mitochondrial membrane potential (MMP) was examined. The mitochondrial membrane potential was measured by adopting fluorescent probe JC-1 specifically labeled mitochondria. The changes in membrane potential were reflected by the ratio of red fluorescence (595 nm) and green fluorescence (525 nm) change of JC-1 (Fig.S10). Treatment with 0, 1 μM and 4 μM of both Mn_1 and Mn_1@GO for 36 h led to MMP collapse, showing reduced red intensity of JC-1. Results suggest that both Mn_1 and Mn_1@GO can enter into negatively charged cells driven by the membrane potential. Cancer cells exhibit an extensive metabolic reprogramming that renders them more susceptible to mitochondrial perturbations [15]. Mitochondria of cancer cells are structurally and functionally different from normal cells such as molecular composition of the mitochondrial inner membrane and the occurrence of mitochondrial membrane permeabilization [16]. Dysfunction of mitochondrial involved in the apoptotic process and the energy metabolism of malignant cell [17]. Hence, we suggest that the good anticancer property of Mn_1 and Mn_1@GO may be the dysfunction of mitochondria.

Fig. 9. Fluorescence image of Mn_1 (10 μM) in HepG-2 cells. a: Mn_1 imaging; b: MitoTracker Red FM imaging; c: Overlapped imaging of Mn_1 and MitoTracker Red FM.

Oxygen is an important factor to maintain cell life and the final electron acceptor in oxidative phosphorylation for energy production [18]. Hypoxia-inducible factor (HIF) regulates the energy metabolism by triggering a switch from mitochondrial oxidative phosphorylation to anaerobic glycolysis [19]. HIF is a common link between O_2 availability, malignant progression, and changes in cancer metabolism. Mn_1 can target mitochondria and react with H_2O_2 or water generating dioxygen, it may have some effect on the expression of HIF-1α in HepG-2 cells. Experimental results show that the content of HIF-1α decreased with the increased concentration of Mn_1, and 30 μM of Mn_1 obviously decreases the expression of HIF-1α in 24 h (Fig. 10). Therefore, this result demonstrates that Mn_1 is a multifunctional complex to attenuate the expression of HIF-1α in cancer cells.

Fig. 10. The expression of HIF-1α in HepG-2 cells after incubated with different concentrations of Mn_1 for 24 h. Control (10 μM DMSO).

4. Conclusions

In normal conditions, both Mn_1 and Mn_1@GO were active against HepG-2 cells, with IC_{50} values of 10.45 μM and 10.14 μM respectively. It was also found that both compounds could be used as photo-activated anticancer materials since Mn_1 (1 μM) and Mn_1@GO (C_{Mn1}, 1 μM) were able to exhibit inhibition on the proliferation of HepG-2 cells when irradiated with green LED light. In particular, Mn_1@GO can react with H_2O_2 resulting active species, and work as H_2O_2 and light activated anticancer nanoparticles. Our results indicate that photoactive Mn(II) complexes loaded GO can be potential both light and H_2O_2 enhanced anticancer agents. In particular,

Mn_1@GO can be LED light enhanced anticancer materials in hypoxic environments and Mn_1 can target mitochondria and has some effect on the expression of HIF-1α in HepG-2 cells. Therefore, this result demonstrates that Mn_1 is a multifunctional complex to attenuate the expression of HIF-1α in cancer cells. Cancer cells use O_2 to generate excessive levels of ROS and H_2O_2. H_2O_2-activatable and O_2-evolving anticancer nanoparticles could be developed further as new kinds of cancer targeted anticancer agents.

Acknowledgments

Financial support from National Science Foundation of China (21271090, 21571085).

Appendix A. Supplementary data

Supplementary data to this article can be found online at http://dx.doi.org/10.1016/.

References

[1] (a) J.P. Celli, B.Q. Spring, I. Rizvi, C.L. Evans, K.S. Samkoe, S. Verma, B.W. Pogue, T. Hasan, Chem. Rev. 110 (2010) 2795−2838. (b) S. Yano, S. Hirohara, M. Obata, Y. Hagiya, S. Ogura, A. Ikeda, H. Kataoka, M. Tanaka, T, Joh, J. Photochem. Photobiol. C. 12 (2011**)** 46-67. (c) P.M. Antoni, A. Naik, I. Albert, R. Rubbiani, S. Gupta, P. Ruiz-Sanchez, P. Munikorn, J.M. Mateos, V. Luginbuehl, P. Thamyongkit, U. Ziegler, G. Gasser, G. Jeschke, B. Spingler, Chem. Eur. J. 21 (2015) 1179-1183.

[2] (a) B.W. Henderson, V.H. Fingar, Cancer Res. 47 (1987) 3110-3114. (b) H.C. Chen, J.W. Tian, W.J. He, Z.J. Guo, J. Am. Chem. Soc. 137 (2015) 1539-1547.

[3] (a) J.M. Brown, W.R. Wilson, Nat. Rev. Cancer. 4*(*2004) 437-447. (b) S.S. Lucky, K.C. Soo, Y. Zhang, Chem. Rev. 115 (2015) 1190-2042.

[4] (a) J.F. Lovell, T.W.B. Liu. J. Chen, G. Zheng, Chem. Rev. 110 (2010) 2839-2857. (b) C.H. Wu, Q.H. He, A.N. Zhu, D. Li, M. Xu, H. Yang, Y.Y. Liu, ACS Appl. Mater. Interfaces 6 (2014) 21615−21623. (C) X. L. Tu, L. Wang, Y. H. Cao, Y.F. Ma, H. Shen, H. M. X. Zhang, Z. J. Zhang, Carbon 97 (2016) 35-44.

[5] M. López-Lázaro, Cancer Lett. 252 (2007) 1-8.

[6] (a) I.S. Turan, F.P. Cakmak, D.C. Yildirim, R. Cetin-Atalay, E.U. Akkaya, Chem. Eur. J. 20 (2014) 16088-16092. (b) Z.W. Wang, Q.Y. Chen, Q.S. Liu, Trans. Metal. Chem. 39 (2014**)** 917-924. (c) D.F. Zhou, Q.Y. Chen, Y. Qi, H.J. Fu, Z. Li, K.D. Zhao, J. Gao, Inorg. Chem. 50 (2011) 6929-6937. (c) Q.Y. Chen, D.F. Zhou, J. Huang, W.J. Guo, J. Gao, J. Inorg. Biochem. 104 (2010) 1141-1147.

[7] J. Liu, W.J. Guo, J. Li, X. Li, J. Geng, Q.Y. Chen, J. Gao, Int. J. Mol. Med. 35 (2015) 607-616.

[8] S. Guo, L.H. Ma, J.Z. Zhao, B. Kuçukoz, A. Karatay, M. Hayvali, H.G. Yaglioglu, Chem. Sci. 5 (2014) 489-500.

[9] (a) C.C. Zhao, Y.F. Zhang, X.Z. Wang, J. Cao, J. Photochem. Photobiol. A: Chem. 264 (2013) 41–47. (b) A. Kamkaew, S.H. Lim,H.B. Lee, L.V. Kiew, L.Y. Chung, K. Burgess, Chem. Soc. Rev. 42 (2013) 77-88.

[10] Q.Y. Chen, M.Y. Kong, P.D. Wang, S.C. Meng, X.L. Xu, RSC Adv. 4(2014) 50693-50698.

[11] (a) Y.N. Ni, F.Y. Zhang, S. Kokot, Anal. Chim. Acta. 769 (2013) 40-48. (b) Y.Q. Xu, A. Malkovskiy, Y.A. Pang, Chem. Comm. 47 (2011) 6662-6664.

[12] Z. Li, Q.Y. Chen, P.D. Wang, Y. Wu, RSC Adv. 3 (2013) 5524-5528.

[13] P. Geijer, S. Peterson, K.A. Åhrling, Z. Deák, S. Styring, Biochim. Biophys. Acta. 1503 (2001) 83-95.

[14] A.T.Y. Lau, Y.Wang, J.F. Chiu, J. Cell. Biochem. 104 (2008) 657-667.

[15] S.J. Ralph, S. Rodríguez-Enríquez, J. Neuzil, R. Moreno-Sánchez, Mol. Aspects Med. 31 (2010) 29-59.

[16] M. López-Lázaro, Mol. Med. 16 (2010) 144 -153.

[17] G.G.M. D'Souza, M.A. Wagle, V. Saxena, A. Shah, Biochem. Biophy. Acta 1807 (2011) 689-696.

[18] N. Dehne, G. Hintereder, B. Brüne, Exp. Cell. Res. 316 (2010) 1179-1189.

[19] N. God N, M. Kanai, Inter. J. Hematol. 95 (2012) 457-463.

Figure captions

Scheme 1. The structure of BDA.

Fig. 1. UV spectra of BDA (a, 10 μM), Mn_1 (b, 10 μM), GO (c, 28 μg·mL^{-1}) and Mn_1@GO (d, C_{Mn1} 6 μM, C_{GO} 30 μg·mL^{-1}) in MeCN-H_2O (v:v = 2:1).

Fig. 2. Fluorescence spectra of Mn_1 (1.5 μM, DMSO) in the presence of various amount of GO (m_{GO}= 0, 20, 40, 60, 80, 100, 120, 140, 160, 180 μg). The excitation wavelength was 460 nm.

Fig.3. TEM image of GO (left) and Mn_1@GO (right).

Fig.4. a) O_2 production from an aqueous solution containing Mn_1(2 mg) under green LED light(500-600 nm, 10 W) at different pH (☆, aqueous phosphate buffer (PB) solution, pH 7.2; ◆, H_2O; ▲, PB solution, pH 8.5 ; ○, PB solution, pH 4.0); b) The initial rate of O_2 evolution plotted as a function of the concentration of Mn_1. Slop =0.027±0.002 min^{-1}, R^2=0.980.

Fig. 5. X-Band EPR spectrum of recycled Mn_1 in MeCN.

Fig. 6. Cyclic voltammetry curves of solutions of Mn_1@GO (C_{Mn}, 1mM) in dry MeCN (black line), Mn_1@GO in MeCN:H_2O = 6:1 (dashed line) at 298 K (vs SCE), platinum working electrode, 100 mV/s scan rate.

Fig. 7. Inhibition activities of Mn_1 and Mn_1@GO on the proliferation of HepG-2 cells. HepG-2 cells without compounds were used as controls.

Fig. 8. Effect on the ROS content in HepG-2 for Mn_1 (1 μM) and Mn_1@GO (C_{Mn1}, 1 μM).

Fig. 9. Fluorescence image of Mn_1 (10 μM) in HepG-2 cells. a: Mn_1 imaging; b: MitoTracker Red FM imaging; c: Overlapped imaging of Mn_1 and MitoTracker Red FM.

Fig. 10. The expression of HIF-1α in HepG-2 cells after incubated with different concentrations of Mn_1 for 24 h. Control (10 μM DMSO).

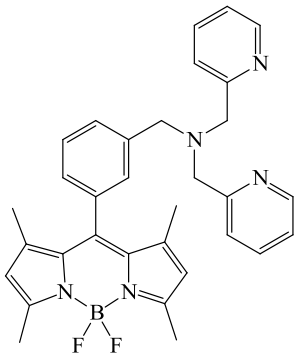

Scheme 1. The structure of BDA.

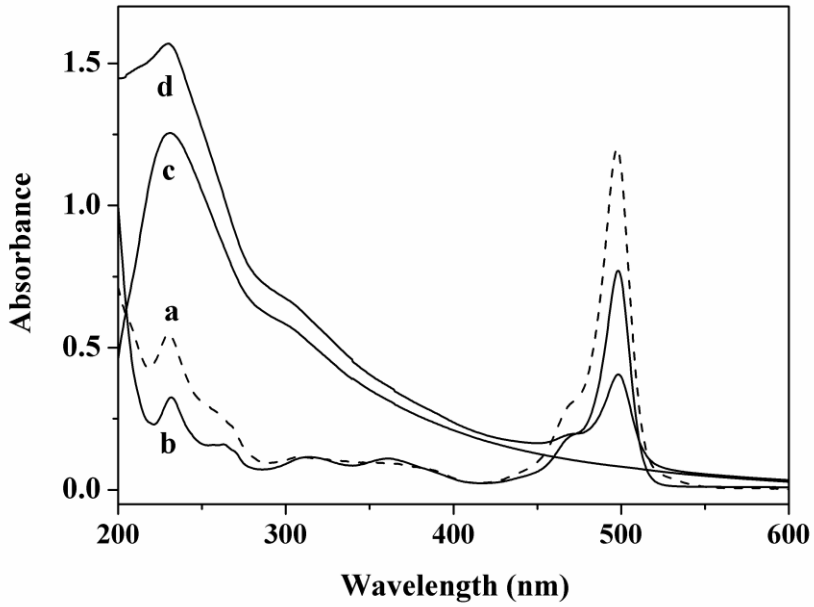

Fig. 1. UV spectra of BDA (a, 10 μM), Mn_1 (b, 10 μM), GO (c, 28 μg·mL^{-1}) and Mn_1@GO (d, C_{Mn1} 6 μM, C_{GO} 30 μg·mL^{-1}) in MeCN-H_2O (v:v = 2:1).

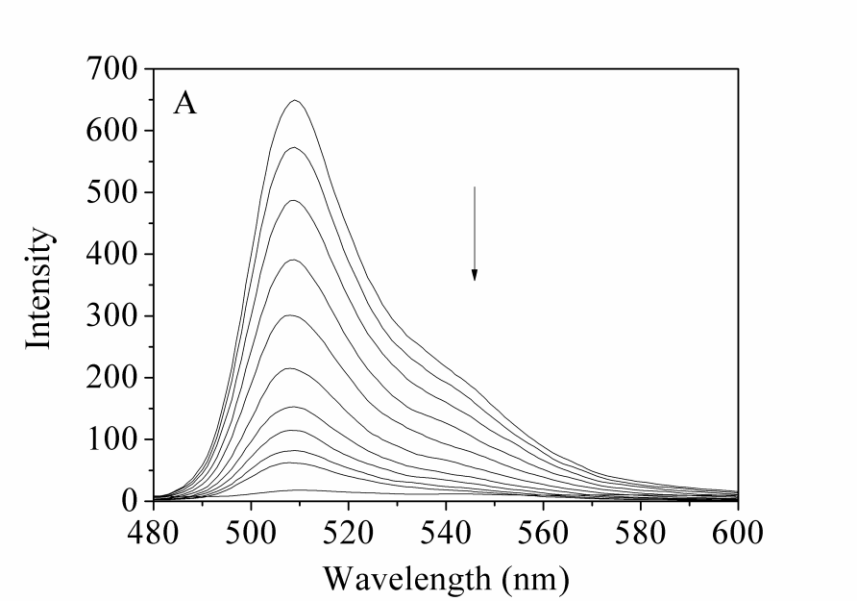

Fig. 2. Fluorescence spectra of Mn_1 (1.5 μM, DMSO) in the presence of various amount of GO (m_{GO}= 0, 20, 40, 60, 80, 100, 120, 140, 160, 180 μg). The excitation wavelength was 460 nm.

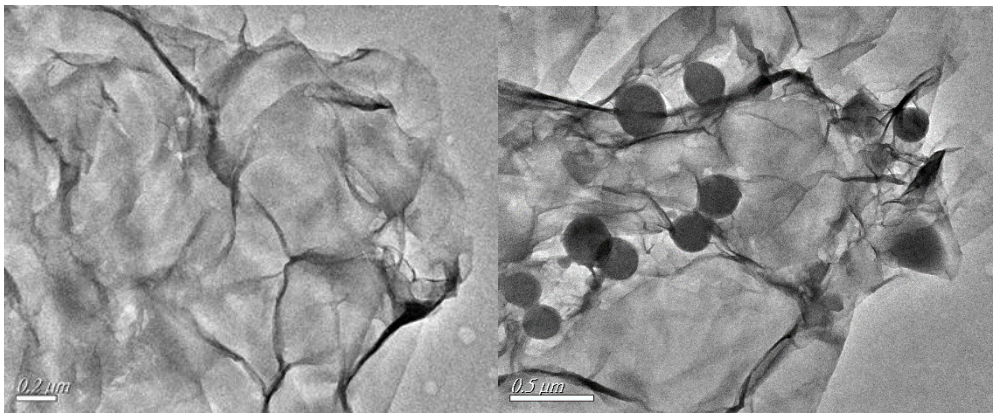

Fig.3. TEM image of GO (left) and Mn_1@GO (right).

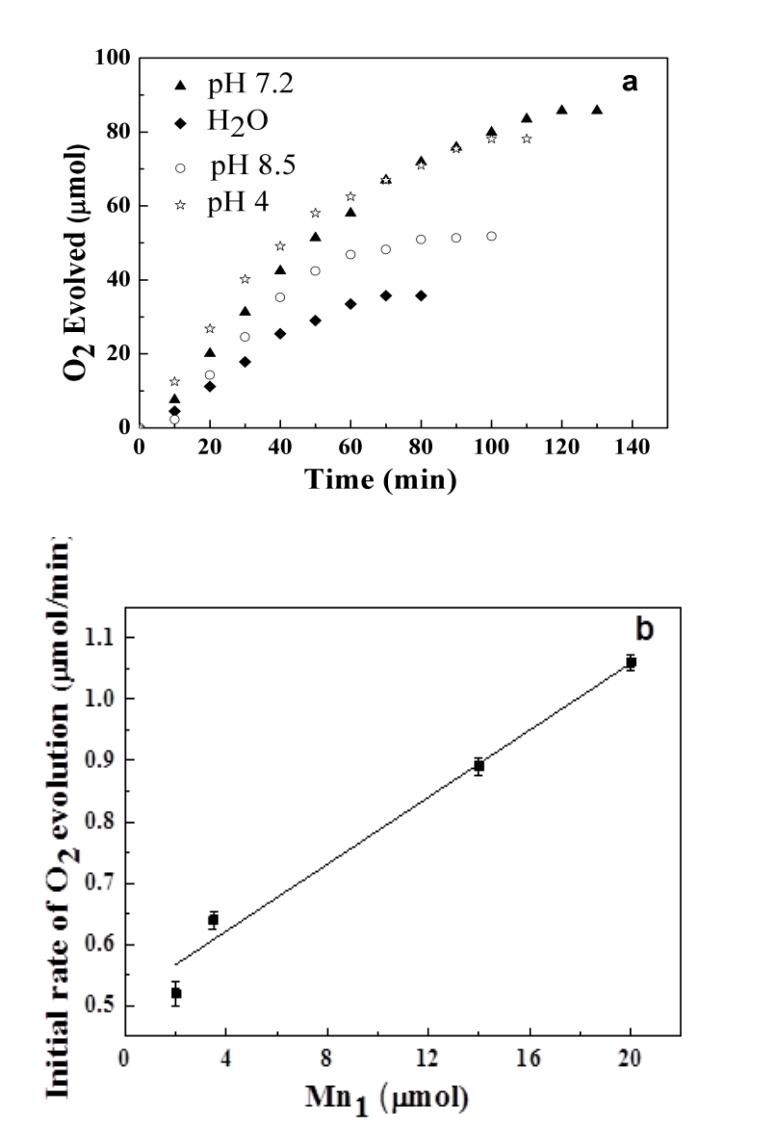

Fig.4. a) O_2 production from an aqueous solution containing Mn_1(2 mg) under green LED light(500-600 nm, 10 W) at different pH (☆, aqueous phosphate buffer (PB) solution, pH 7.2; ◆, H_2O; ▲, PB solution, pH 8.5 ; ○, PB solution, pH 4.0); b) The initial rate of O_2 evolution plotted as a function of the concentration of Mn_1. Slop =0.027±0.002 min^{-1}, R^2=0.980.

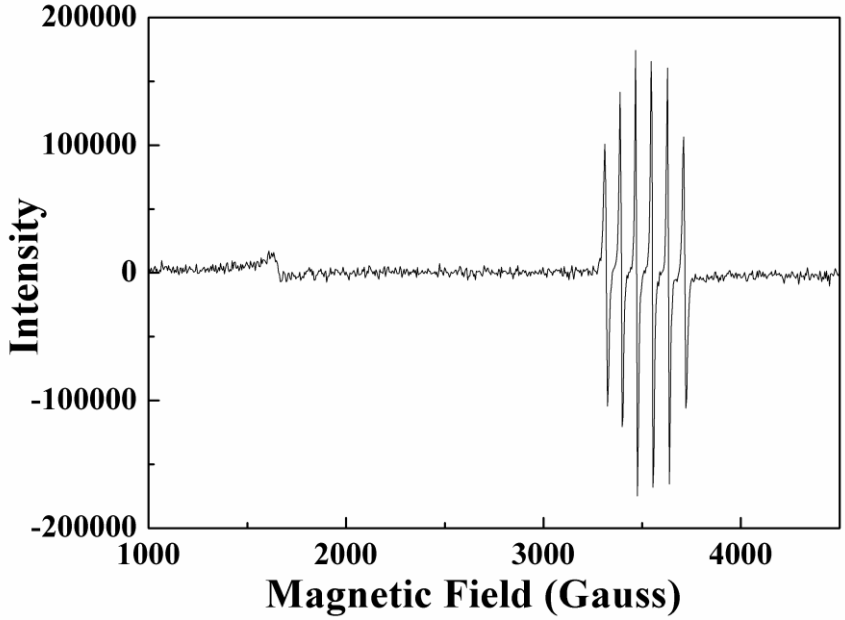

Fig. 5. X-Band EPR spectrum of recycled Mn_1 in MeCN

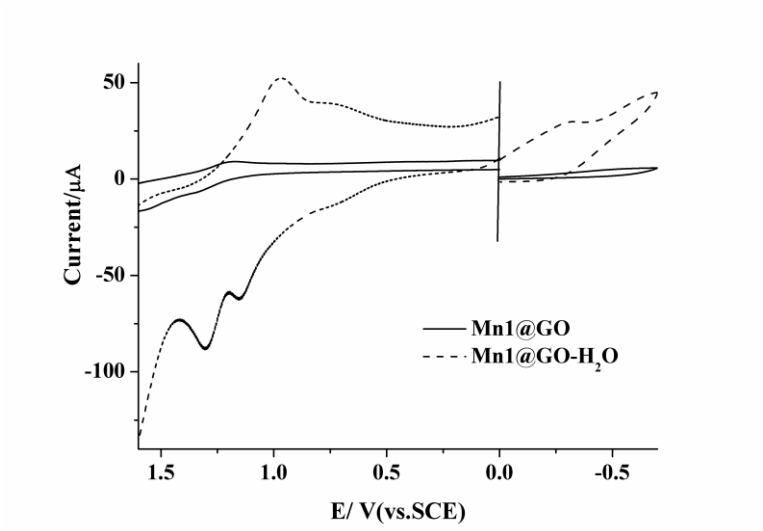

Fig. 6. Cyclic voltammetry curves of solutions of Mn_1@GO (C_{Mn}, 1mM) in dry MeCN (black line), Mn_1@GO in MeCN:H_2O = 6:1 (dashed line) at 298 K (vs SCE), platinum working electrode, 100 mV/s scan rate.

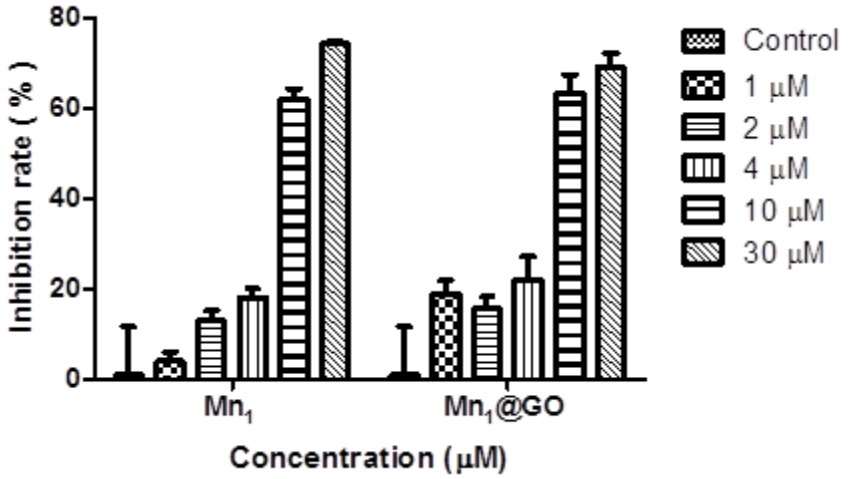

Fig. 7. Inhibition activities of Mn_1 and Mn_1@GO on the proliferation of HepG-2 cells. HepG-2 cells without compounds were used as controls.

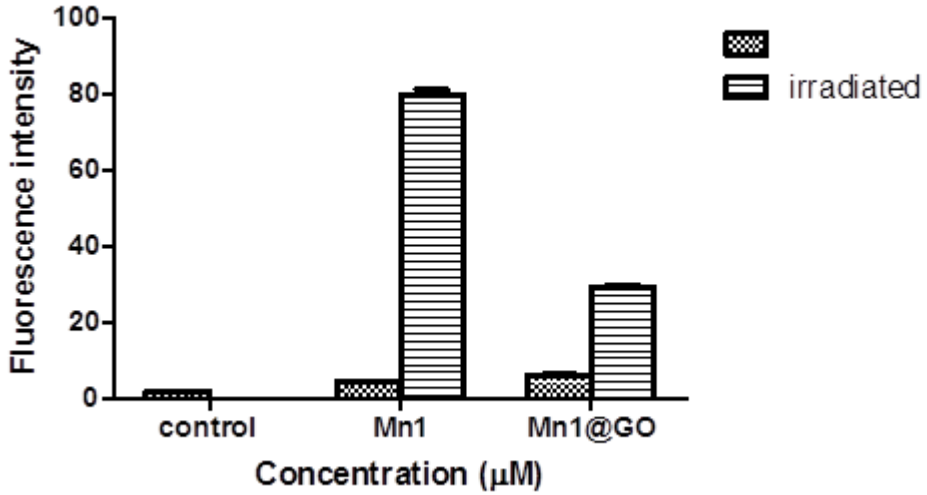

Fig. 8. Effect on the ROS content in HepG-2 for Mn_1 (1 μM) and Mn_1@GO (C_{Mn1}, 1 μM).

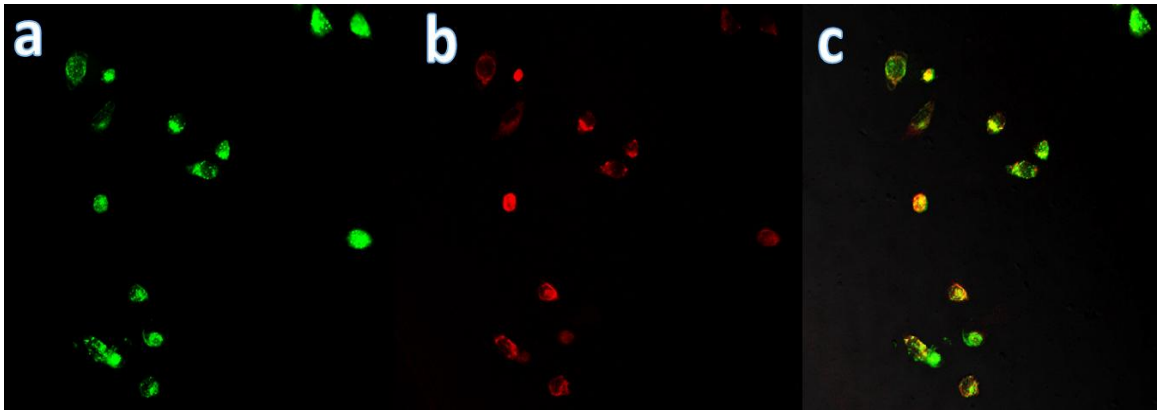

Fig. 9. Fluorescence image of Mn_1 (10 μM) in HepG-2 cells. a: Mn_1 imaging; b: MitoTracker Red FM imaging; c: Overlapped imaging of Mn_1 and MitoTracker Red FM.

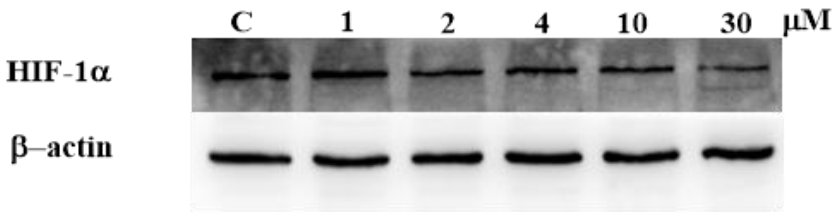

Fig. 10. The expression of HIF-1α in HepG-2 cells after incubated with different concentrations of Mn_1 for 24 h. Control (10 μM DMSO).